Effects of temperature and grain size on diffusivity of aluminium electromigration experiment and molecular dynamic simulation

Cui, Zhen; Zhang, Yaqian; Hu, Dong; Vollebregt, Sten; Fan, Jiajie; Fan, Xuejun; Zhang, Guoqi

DOI
10.1088/1361-648X/ac4b7f

Publication date
2022

Document Version
Final published version

Published in
Journal of physics. Condensed matter : an Institute of Physics journal

PAPER

Effects of temperature and grain size on diffusivity of aluminium: electromigration experiment and molecular dynamic simulation

To cite this article: Zhen Cui *et al* 2022 *J. Phys.: Condens. Matter* **34** 175401

IOP Publishing Journal of Physics: Condensed Matter
J. Phys.: Condens. Matter **34** (2022) 175401 (13pp) https://doi.org/10.1088/1361-648X/ac4b7f

Effects of temperature and grain size on diffusivity of aluminium: electromigration experiment and molecular dynamic simulation

Zhen Cui[1,4], Yaqian Zhang[1,4], Dong Hu[1], Sten Vollebregt[1], Jiajie Fan[2], Xuejun Fan[3,*] and Guoqi Zhang[1,*]

[1] Department of Microelectronics, Delft University of Technology, 2628 CD, Delft, The Netherlands
[2] Academy for Engineering & Technology, Fudan University, Shanghai, 200433, People's Republic of China
[3] Department of Mechanical Engineering, PO Box 10028, Lamar University, Beaumont, TX 77710, United States of America

E-mail: xfan@lamar.edu and g.q.zhang@tudelft.nl

Received 25 November 2021, revised 22 December 2021
Accepted for publication 14 January 2022
Published 25 February 2022

Abstract

Understanding the atomic diffusion features in metallic material is significant to explain the diffusion-controlled physical processes. In this paper, using electromigration experiments and molecular dynamic (MD) simulations, we investigate the effects of grain size and temperature on the self-diffusion of polycrystalline aluminium (Al). The mass transport due to electromigration are accelerated by increasing temperature and decreasing grain size. Magnitudes of effective diffusivity (D_{eff}) and grain boundary diffusivity (D_{GBs}) are experimentally determined, in which the D_{eff} changes as a function of grain size and temperature, but D_{GBs} is independent of the grain size, only affected by the temperature. Moreover, MD simulations of atomic diffusion in polycrystalline Al demonstrate those observations from experiments. Based on MD results, the Arrhenius equation of D_{GBs} and empirical formula of the thickness of grain boundaries at various temperatures are obtained. In total, D_{eff} and D_{GBs} obtained in the present study agree with literature results, and a comprehensive result of diffusivities related to the grain size is presented.

Keywords: effective diffusivity, grain boundary diffusivity, electromigration, molecular dynamic simulation

(Some figures may appear in colour only in the online journal)

1. Introduction

Atomic diffusion in polycrystalline metals is a basic physical phenomenon that broadly affects the performance of metallic materials in practical applications. Essentially, the self-diffusion coefficient plays a significant role in quantitatively analyzing and predicting some physical processes in metals, such as electromigration [1–4], Coble creep [5–8], nanoparticle sintering [9–12], and recrystallization [13].

Determination of atomic diffusivity is not a straightforward work. Over the past decades, various experimental methods have been proposed to determine the diffusivity in metals. One of the most reliable methods is the aid of tracer sectioning techniques by means of radioactive isotopes [14]: (1) depositing a thin layer of radiotracers on the flat surface of sample.

* Authors to whom any correspondence should be addressed.
[4] Zhen Cui and Yaqian Zhang equally contribute to present work.

(2) Heating the sample to a high temperature, at least half of the melting temperature, to promote the atomic diffusion. (3) After a certain time, by using the methods of sectioning, the depth of tracer diffused in sample can be measured. (4) According to the diffusion model of thin film, atomic diffusivity is determined. Moreover, the methods of nuclear magnetic resonance (NMR) and quasi-elastic neutron scattering (QNS) were developed to determine the diffusivity in metals [15, 16]. As one example relevant to this work, table 1 summarizes the data for self-diffusion in Al. For the 'average' diffusivity, also called effective diffusivity (D_{eff}), Seeger *et al* [15] investigated the temperature dependence of mass transport in Al by using the tracer and NMR techniques. They determined an Arrhenius equation with the pre-exponential $D_0 = 0.047\ \text{cm}^2\ \text{s}^{-1}$ and activation energy $E_a = 1.26$ eV. Moreover, Lundy and Murdock [17] determined that the activation energy of D_{eff} in Al is 1.47 eV using the radioactive Al [26]. However, in the study conducted by Demmel *et al* [16], a much lower activation energy was determined to be 0.274 eV by using coherent QNS technique.

For the mass transport in polycrystalline, grain boundaries (GBs) provide a fast-diffusion path [18, 19]. Experimental methods to determine the GBs diffusivity (D_{GBs}) can be divided into two categories, direct and indirect methods. In direct measurements [20, 21], D_{GBs} is extracted from the penetration profile (concentration vs depth) of radioactive tracer diffused into a polycrystal containing GBs. The penetration profile is analysed in terms of continuum models, in which GBs are represented by a 2D 'path' with thickness δ_{GBs} whose diffusivity is much larger than the lattice diffusivity. By fitting the mathematical solutions to the experimental profile, the 'average' atomic diffusivity in grain boundary can be determined. In indirect methods, D_{GBs} can be calculated from the rate of a particular diffusion-controlled process, such as internal friction [22], electromigration [23], and void growth kinetics [24]. Essentially, it can be any process whose rate is assumed to be controlled by GBs diffusion and for which a model containing D_{GBs} is available. Table 1 shows the experimental data for D_{GBs} in Al in literature. Only indirect measurements from the kinetics of film deposition and electromigration are available.

Atomistic modelling, as an effective tool to investigate the material properties at the atomic-level, provides a new way to calculate diffusivities in metals. Sandberg *et al* [25] calculated the self-diffusion coefficient in Al by using first-principles calculation. Jakse and Pasturel [26] investigated the atomic diffusion in liquid Al using density-functional theory. But, as the expensive cost in first-principles calculations, above mentioned simulations were carried out using small models without considering the effect of GBs. Recently, molecular dynamics (MD) simulation has been shown to be able to study the material properties related to the GBs. Suzuki and Mishin [27] investigated the atomic diffusion along Cu GBs using the MD simulation, identifying that vacancies migrate along GBs by exchanging positions with individual atoms. In the study conducted by Sorensen *et al* [37], the atomic diffusivity along Cu GB $\sum = 5(210)$ was discovered to follow the Arrhenius law quite accurately over a wide range of temperatures. Furthermore, using MD simulation, Mohammadzadeh *et al* [28] studied the effects of structure and geometry of GBs on the diffusion kinetics in nanocrystalline Al, in which the influence of GBs misorientation on the diffusion coefficient was investigated. Arrhenius equation for the diffusivity in Al symmetric tilt GBs was obtained as listed in table 1.

As mentioned above, different results of the atomic diffusivity in Al appeared in literatures, which confuses the selection of atomic diffusivity for the study of diffusion-related physical phenomena. Moreover, there is a lack of comprehensive experimental study to quantitatively investigate the effect of grain size on the atomic diffusivity of Al. In this paper, a systematic study of atomic diffusion in columnar polycrystalline Al is presented by using experimental and simulation methods. Using the electromigration, the mass transport process in Al with various grain sizes at different temperatures is conducted. According to the experimental results and electromigration theory, D_{eff} and D_{GBs} are determined accordingly. Moreover, diffusion behaviours for atom motion along GBs are studied by using the MD simulation. The calculated D_{GBs} are compared with present experimental results, and an Arrhenius equation for the D_{GBs} is determined. Lastly, the effects of grain size and temperatures on D_{eff} and D_{GBs} are analyzed and compared with literature results.

2. Methodology

2.1. Electromigration experiment procedure

2.1.1. Sample fabrication. Following the Blech's structure [3, 18], samples with Al as the testing metal film, TiN as the interlayer, and SiO_2/Si as the substrate are fabricated. The details of sample fabrication are given in reference [38], and they are briefly described here for continuity. Fabrication started with the growth of 200 nm SiO_2 by thermal oxidation on a silicon wafer, which is intended as an etching-stopping layer and thermal isolated layer. After thermal oxidation, a 300 nm TiN layer was deposited on SiO_2 layer by using sputtering method. Subsequently, 200 nm thick Al films were deposited on TiN using RF sputtering method at 25 °C, 300 °C, and 400 °C. Finally, the Al films were etched to pattern structures using the wet etching method. In this sample, as the Al is a better conductor than TiN, thus the current will detour from the TiN to Al to guarantee the electromigration occurring in Al stripes. Figure 1(a) shows fabricated Al stripes with lengths of 10 μm, 30 μm, 60 μm, and 100 μm. The width of all Al stripes is 5 μm.

2.1.2. Measurement setup and testing procedure. A schematic overview of the electromigration measurement setup is illustrated in figure 1(b), which is consists of a Nextron MPS-CHH microprobe chamber with a ceramic chuck. This chamber could be pumped down, while electrical measurements could be performed using four available probe needles with 20 μm rhodium coated tips. A temperature controller could heat the chamber from 50 °C to 750 °C. The vacuum was arranged via a Boc Edwards XDS-10 scroll

Table 1. Summary of experimental data for the pre-exponential factor D_0 and activation energy E_a of D_{eff} and D_{GBs} in Al. The dash indicates that data is unavailable.

	Effective diffusivity		Grain boundary diffusivity		
Literature	D_0 (m^2 s^{-1})	E_a (eV)	D_0 (m^2 s^{-1})	E_a (eV)	Method
Seeger *et al* [15]	4.7×10^{-6}	1.26	—	—	Tracer and NMR
Lundy and Murdock [17]	1.71×10^{-4}	1.47	—	—	Radioactive isotopes
Demmel *et al* [16]	—	0.27	—	—	Coherent QNS
Kargl *et al* [29]	—	0.28	—	—	Incoherent QNS
Fradin and Rowland [30]	3.50×10^{-6}	1.23	—	—	NMR
Stoebe and Dawson [31]	2.0×10^{-6}	1.22	—	—	NMR
Volin and Balluffin [32]	1.76×10^{-5}	1.31	—	—	Void shrinkage kinetics
Burke *et al* [33]	0.19×10^{-4}	1.28	—	—	Dislocation climb
Levenson [34]	—	—	—	0.55	Film deposition kinetics
Schreiber and Grabe [35]	—	—	—	0.47	Electromigration
Wang *et al* [36]	—	—	$3.2–16.2 \times 10^{-16}$	—	Electromigration
Sandberg *et al* [25]	—	1.43	—	—	First principles calculation
Jakse and Pasturel [26]	—	0.25	—	—	First principles calculation
Mohammadzadeh *et al* [28]	—	—	$2.3–6.9 \times 10^{-10}$	0.44–0.61	MD simulation

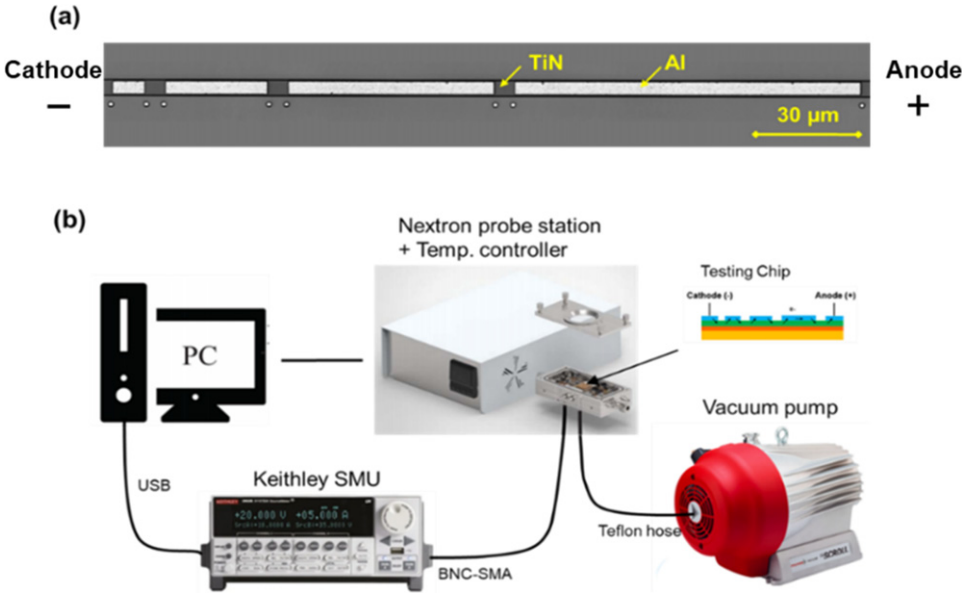

Figure 1. (a) Top view of the sample used in electromigration test. (b) A schematic overview of the electromigration measurement setup.

pump. Current loading was provided using a Keithley 2612B source measure unit. The temperature, current loading, and duration of the testing were controlled using a personal computer (PC).

In present measurements, Al stripes deposited at 25 °C, 300 °C, and 400 °C were respectively tested under a current density of 1×10^{10} MA cm^{-2} in the vacuum chamber. Temperatures of 200 °C, 250 °C, 300 °C, and 350 °C were maintained via the heater at the substrate. After measurements, Keyence VK-X250 and SEM Hitachi Regulus 8230 were used to characterize the results of electromigration.

2.2. Molecular dynamic simulation details

Present MD simulations were conducted using the large-scale atomic/molecular massively parallel simulator. The embedded-atom method with potential file developed by Voter was used to calculate the interaction between Al atoms [39]. This potential has been proven to accurately calculate the atomic diffusion property, lattice parameters, and GBs of Al [40, 41]. Newton's equation of motion was integrated with the Verlet algorithm. The timestep of 2 fs was chosen for calculation and the periodic boundary condition was applied in the three dimensions. Polycrystalline Al with grain sizes of ∼25 nm, ∼20 nm, ∼14 nm, and ∼10 nm were constructed using the Voronoi method [42, 43], as illustrated in figures 2(a)–(c). The green region represents the atoms in grains with fcc lattice structure and the grey region represents the atoms in GBs with the irregular lattice structure. There were three random polycrystalline structures at each level of grain size. The dimensions of the model along the x, y, and z directions were 400 Å, 400 Å, and 100 Å, respectively.

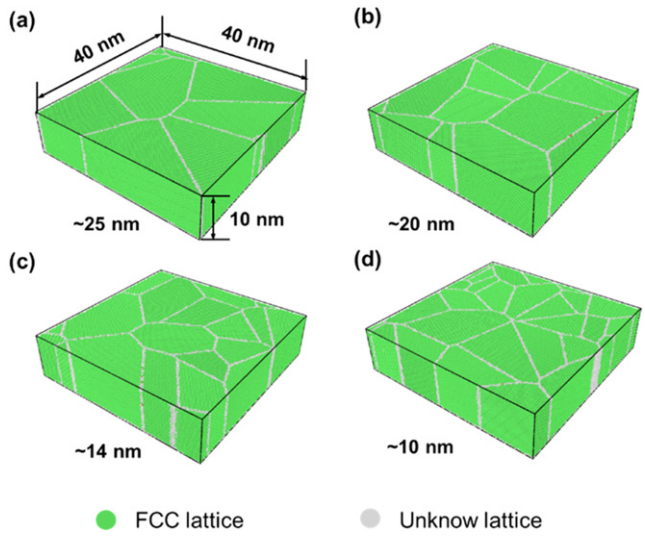

Figure 2. Polycrystalline models with grain sizes of (a) 25 nm, (b) 20 nm, (c) 14 nm, and (d) 10 nm. The green region represents the atoms in grains with fcc lattice structure and the grey region represents the atoms in GBs with the irregular lattice structure.

The total number of atoms was approximately one million. The open visualization tool (OVITO) software was used to visualize our simulation results [44].

The atomic diffusivities were calculated via four steps: (1) system energy was minimized. The coordinates of the atoms were iteratively adjusted until the change in energy between outer iteration was less than 1×10^{-8} eV Å^{-1} (2) after that, the system was relaxed for 1500 ps in the NPT ensemble with the target temperatures (300 K, 400 K, 500 K, 600 K, 700 K) at zero pressure, to obtain a stable microstructure without grain boundary migration. (3) On the basics of fully relaxed structure, the computation of polyhedral template matching was performed with lattice distortion threshold as 0.11. In this step, the atoms with fcc, hcp, bcc, ICO, and sc lattice structures could be identified, and the atoms with unknown lattice structure were defined as atoms along GBs. (4) We continually relaxed the system for 2000 ps to calculate the mean-squared displacement (MSD) and diffusivities for atoms in GBs and the entire models. Here, the MSDs were computed by using the following equations [10, 45],

$$\mathrm{MSD}_{\mathrm{GBs}} = \frac{1}{N_{\mathrm{GBs}}} \sum_{i=1}^{N} [r_i(t) - r_i(0)]^2 \tag{1}$$

$$\mathrm{MSD}_{\mathrm{eff}} = \frac{1}{N_{\mathrm{all}}} \sum_{i=1}^{N} [r_i(t) - r_i(0)]^2 \tag{2}$$

where N_{GBs} and N_{all} mean the number of atoms in GBs and the entire model, respectively. $r_i(t)$ and $r_i(0)$ are the positions of atom i at time t and 0. Based on the calculated MSDs, the diffusivity in solid material can be calculated via the following Einstein relation [45–47],

$$D_{\mathrm{GBs}} = \lim_{t\to\infty} \frac{1}{2n} \frac{\mathrm{dMSD}_{\mathrm{GBs}}}{\mathrm{d}t} \tag{3}$$

$$D_{\mathrm{eff}} = \lim_{t\to\infty} \frac{1}{2n} \frac{\mathrm{dMSD}_{\mathrm{eff}}}{\mathrm{d}t} \tag{4}$$

where n is the dimension of the simulation structure, which is equal to 3 for the present three-dimension model. Although the time period used in the MD calculation of diffusivity was only a few nanoseconds, existing studies [45, 47, 48] have proven that the MD simulation is able to calculate the atomic diffusivity accurately.

3. Experiment results and discussions

Figure 3 shows the electromigration results for 300 °C-deposited Al stripes at 250 °C. Voids at cathode and hillock at anode were observed, which is a typical failure phenomenon due to atoms diffuse from cathode to anode. Moreover, the void size increases with the increasing stripe length and time, which is consistent with observations in literature. For the 10 μm conductor, void is very small and stops growing after 8 h. Obviously, a critical length to balance electromigration around 10 μm was indicated. Mechanisms behind those phenomena will be explained in section 3.3.

3.1. Effect of temperature

Figure 4 shows the electromigration results for 300 °C-deposited Al stripes at various temperatures. From 200 °C to 350 °C, void sizes in 30–100 μm stripes increase with the increasing temperature. This indicates that the atomic diffusion under higher temperature develops faster. Moreover, there was almost no void in 10 μm Al stripes at all temperatures. Thus, the critical length to stop electromigration seems to be little affected by temperature in the range from 200 °C to 350 °C.

For the electromigration results measured using 25 °C-deposited Al stripes under 1 MA cm^{-2}, figure 5 shows the similar changing trend—void size increases with increasing temperature. At 200 °C, small voids were observed in 30/60/100 μm Al stripes. When the temperature increased from 200 °C to 350 °C, more than half of Al stripes were depleted at cathode. Compared to the results shown in figure 4, electromigration development in 25 °C-deposited Al is faster than that in 300 °C-deposited Al. Moreover, from 200 °C to 300 °C, the critical length to stop electromigration is around 10 μm. But, there was a visible void in 10 μm conductor at 350 °C, which indicates that the critical length could be reduced with increasing temperature in 25 °C-deposited samples.

Figure 6 shows the testing results for 400 °C-deposited Al stripes. Evolution of void is qualitatively consistent with the results shown in figures 4 and 5. Void grows faster at a higher temperature. At 200 °C, voids are very small in all stripes, indicating a slight mass transport. With the increasing temperature, the mass transport is accelerated, leading to the increase of void size. Compared to the void sizes in the 25 °C- and 300 °C-deposited Al stripes, the mass transport in 400 °C-deposited Al stripes develops noticeably slower. Moreover, the critical length is also identified to be 10 μm, same to that in 25 °C- and 300 °C-deposited Al stripes. In total, results shown

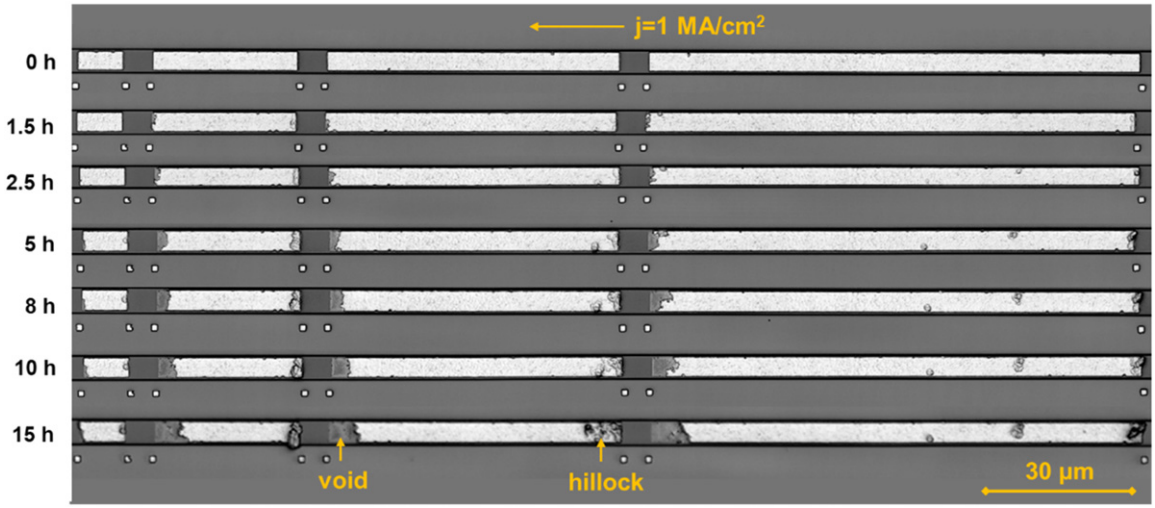

Figure 3. Electromigration results for 300 °C deposited Al stripes with lengths of 10 μm, 30 μm, 60 μm, and 100 μm under 1 MA cm^{-2} at 250 °C from 0 to 20 h.

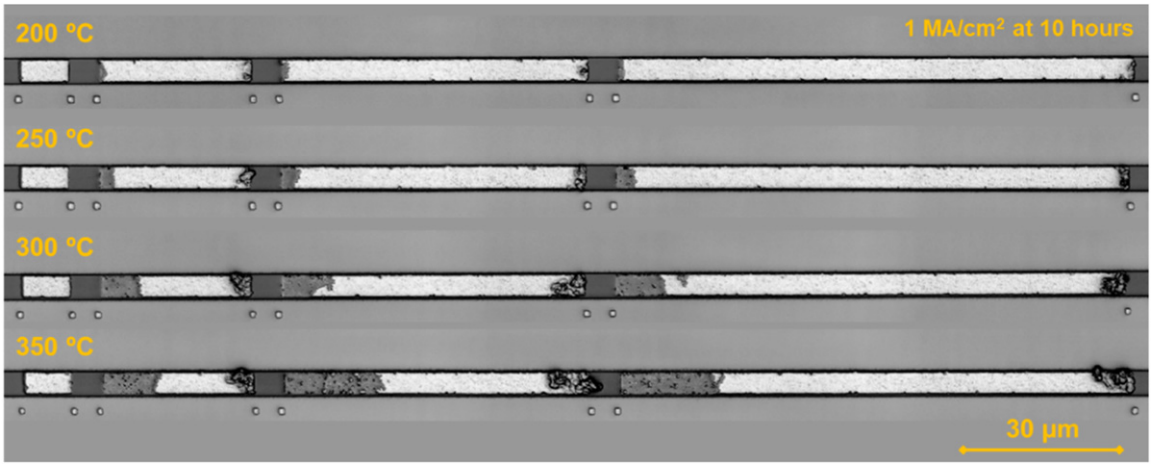

Figure 4. Electromigration results for 300 °C-deposited Al stripes under 1 MA cm^{-2} at 200 °C, 250 °C, 300 °C, and 350 °C at 10 h.

in figures 4–6 repeatedly demonstrate that the increasing temperature can accelerate the mass transport but slightly affect the critical length.

3.2. Effect of grain size

Except for the temperature, the rate of mass transport in Al stripes is noticeably affected by the deposition temperature. As shown in figure 7, under the same testing conditions and duration, voids in 300 °C-deposited Al stripes are obviously smaller than those in 25 °C-deposited Al stripes. And the voids in 400 °C-deposited Al stripes are even smaller. Those results indicate that the increasing deposition temperature can decelerate the development of electromigration. A similar trend is also shown in figure 8 for the samples tested at 350 °C for 10 h. Voids in 25 °C-deposited Al are significantly larger than those deposited at 300 °C and 400 °C, indicating a rapid mass transport in 25 °C-deposited Al. Moreover, the voids in 300 °C-deposited Al are a little bit larger than those in 400 °C-deposited Al, implying a slightly accelerated electromigration using a lower deposition temperature.

Figure 9 shows the SEM images of microstructures in Al stripes deposited at different temperatures. Grain size increases with increasing deposition temperature. At 25 °C, the average grain size in Al is very small, ∼112 nm. When temperature increases to 300 °C and 400 °C, the average grain size grows to 315 nm and 550 nm, respectively. In polycrystalline metals, as the grain boundary acts as a fast diffusion pathway, thus the increase of GBs means a higher diffusion rate of atoms. As illustrated in figure 9, the increase of grain size could cause less GBs, thus the effective diffusion rate in Al tends to decrease with increasing grain size. This is consistent with observations of electromigration results.

3.3. Effective diffusivity and grain boundary diffusivity

3.3.1. Calculation method for diffusivity. Based on the Nernst–Einstein equation [49], the drift velocity of mass

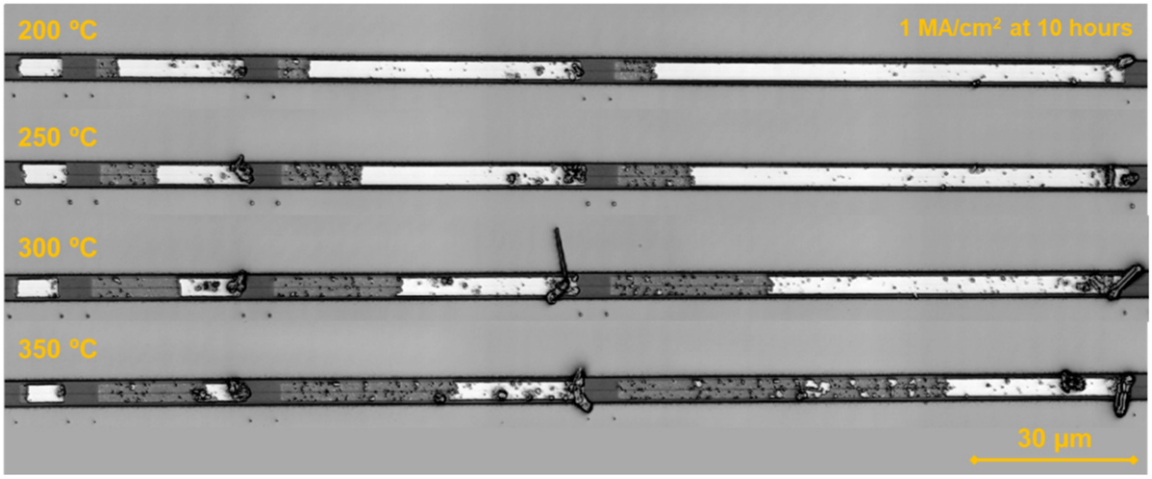

Figure 5. Electromigration results for 25 °C-deposited Al stripes under 1 MA cm^{-2} at 200 °C, 250 °C, 300 °C, and 350 °C at 10 h.

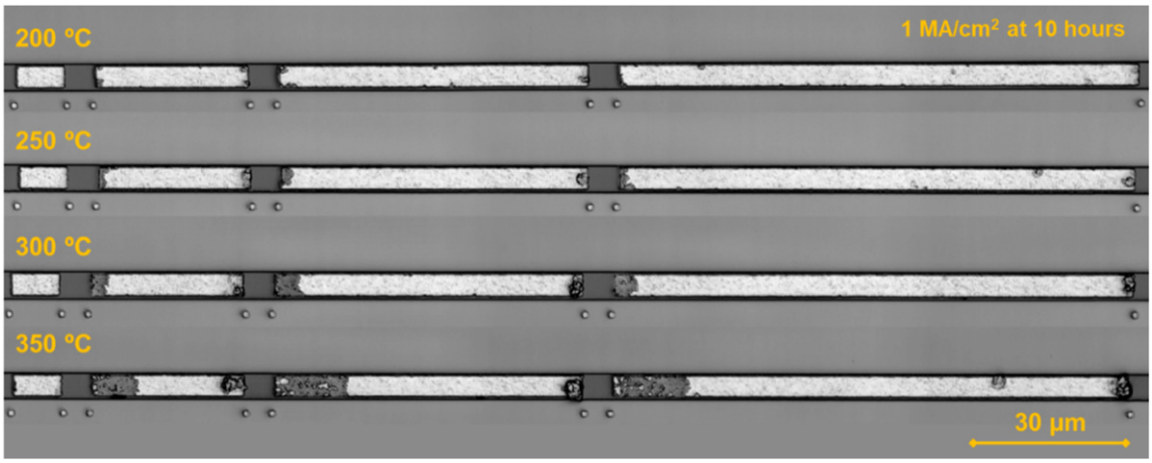

Figure 6. Electromigration results for 400 °C -deposited Al stripes under 1 MA cm^{-2} at 200 °C, 250 °C, 300 °C, and 350 °C at 10 h.

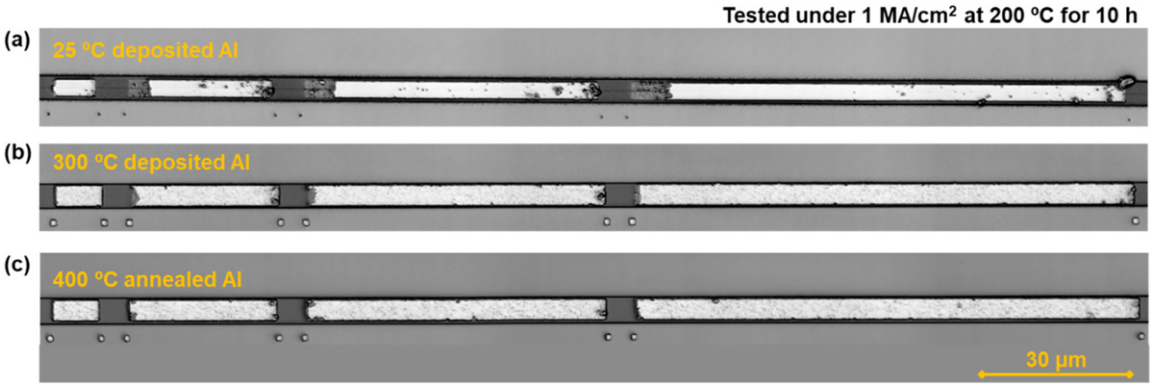

Figure 7. Electromigration results for Al stripes with different deposition temperatures tested under 1 MA cm^{-2} at 200 °C for 10 h.

transport is given as following equation [23],

$$v_{drift} = D_{eff}\frac{F}{kT} \tag{5}$$

where D_{eff} is the effective diffusivity (m^2 s^{-1}). F is the driving force of atomic diffusion (N), which is consist of the electron wind force ($Z^*e\rho j$), the stress gradient ($\Delta\sigma/\Delta L$), the atomic concentration gradient ($\Delta C_a/(C_{a0}\Delta L)$, and the

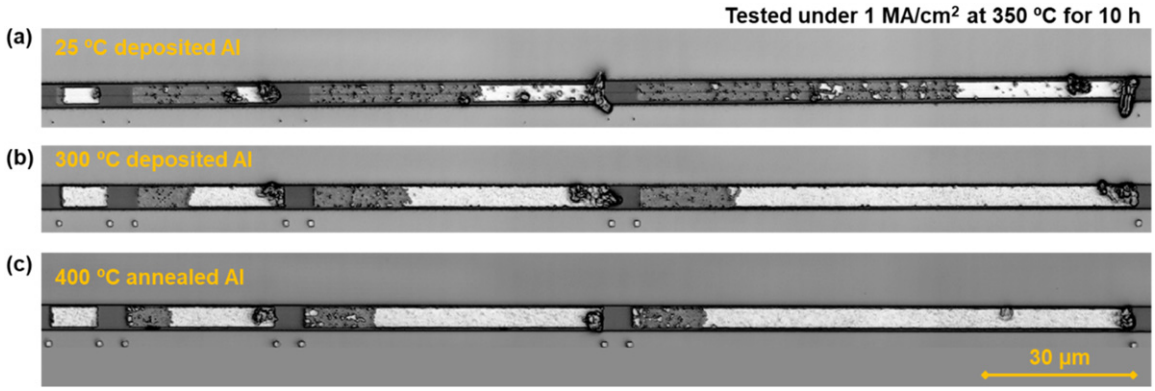

Figure 8. Electromigration results for Al stripes with different deposition temperatures tested under 1 MA cm^{-2} at 350 °C for 10 h.

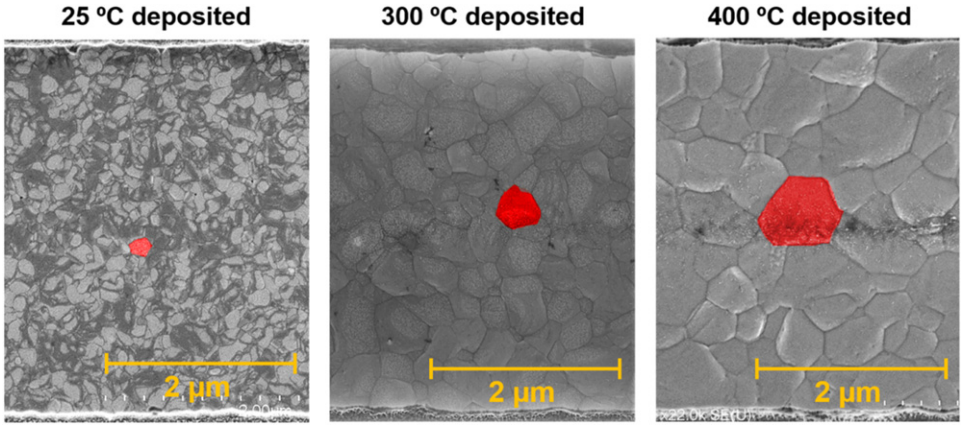

Figure 9. SEM images for Al stripes deposited at 25 °C, 300 °C, 400 °C, respectively.

temperature gradient ($\Delta T/\Delta L$). Thus, above equation can be written as follows,

$$v_{drift} = \frac{D_{eff}}{kT}\left(-Z^* e\rho j - \frac{kT\Delta C_a}{C_{a0}\Delta L} + \frac{\Omega\Delta\sigma}{\Delta L} - Q^*\frac{\Delta T}{T^2\Delta L}\right) \tag{6}$$

where Z^* is the effective charge, e the electronic charge (C), ρ the resistivity (Ohm m), j the current density (A m^{-2}), and Q^* is the heat of transfer (kJ mol^{-1}). For pure Al, the atom motion due to temperature gradient is largely less than electromigration [50, 51]. And, in present study the Al conductor was tested without passivation layer, the effect from mechanical stress is very limited [1]. Therefore, the mass transport in present test is mainly controlled by electron wind and concentration gradient, thus equation (6) is simplified as follows,

$$v_{drift} = \frac{D_{eff}}{kT}\left(-Z^* e\rho j - \frac{kT\Delta C_a}{C_{a0}\Delta L}\right). \tag{7}$$

The void length is equal to the integral of drift velocity over testing time t,

$$L_{void} = \int_0^t v_{drift}\,dt. \tag{8}$$

As illustrated in figure 10, the total length of stripe is the sum of L_{void}, ΔL, and $L_{hillock}$. Present experiments have shown that the $L_{hillock}$ only occupies a small part of total length of 100 μm conductor. Thus, the total length of 100 μm strip can be approximately considered as $L \approx L_{void} + \Delta L$. Moreover, the difference of atomic concentration at both ends is defined as $\Delta C_a = C_{a,hillock} - C_{a,void}$. Combining above equations (5), (7) and (8), we can obtain the following equation,

$$L_{void} = \int_0^t \frac{D_{eff}}{kT}\left[-Z^* e\rho j - \frac{kT\Delta C_a}{C_{a0}(L - L_{void})}\right] dt. \tag{9}$$

When the parameters of L_{void}, L, kT, $Z^*e\rho j$, and t are known, the effective diffusivity can be determined by solving equation (9). Additionally, Hart *et al* [52] provided an equation to describe the relation between D_{eff} and D_{GBs} in bicrystal materials, in which D_{eff} is quantitatively equal to the weighted average of the D_{GBs} and the lattice diffusivity. Recently, Chen *et al* [53] improved Hart's equation to columnar polycrystalline materials as follows,

$$D_{eff} = D_{GBs}\frac{H_{GBs}\delta}{d_{Grain}} \tag{10}$$

where δ is the thickness of GBs, d_{Grain} is the grain size, and H_{GBs} is a dimensionless numerical factor changing from 2.57 to 2.91 for different microstructure of material [54, 55]. Based on equation (10), we can determine the D_{GBs} when D_{eff}, H_{GBs}, δ, and d_{Grain} are known.

Table 2. Void lengths for the 100 μm Al stripes. L_{void} is void length, and t is the duration time.

	25 °C deposited Al stripes		300 °C deposited Al stripes		400 °C deposited Al stripes	
Temperature	L_{void} (μm)	t (h)	L_{void} (μm)	t (h)	L_{void} (μm)	t (h)
200 °C	8.75	10	1.39	10	2.98	30
250 °C	15.35	10	3.75	10	2.09	10
300 °C	33.21	10	9.95	10	4.13	10
350 °C	70.53	10	18.92	10	12.862	10

Table 3. Effective diffusivity (D_{eff}) and GBs diffusivity (D_{GBs}) for various Al stripes tested at different temperatures.

	25 °C deposited Al stripes ~110 nm grain size		300 °C deposited Al stripes ~315 nm grain size		400 °C deposited Al stripes ~550 nm grain size	
Temperature	D_{eff} ($m^2\ s^{-1}$)	D_{GBs} ($m^2\ s^{-1}$)	D_{eff} ($m^2\ s^{-1}$)	D_{GBs} ($m^2\ s^{-1}$)	D_{eff} ($m^2\ s^{-1}$)	D_{GBs} ($m^2\ s^{-1}$)
200 °C	3.95×10^{-14}	1.36×10^{-12}	5.92×10^{-15}	6.43×10^{-13}	4.34×10^{-15}	8.50×10^{-13}
250 °C	7.64×10^{-14}	2.63×10^{-12}	1.83×10^{-14}	1.98×10^{-12}	1.02×10^{-14}	1.99×10^{-12}
300 °C	1.86×10^{-13}	6.41×10^{-12}	5.50×10^{-14}	5.97×10^{-12}	2.24×10^{-14}	4.38×10^{-12}
350 °C	4.68×10^{-13}	1.61×10^{-11}	1.14×10^{-13}	1.23×10^{-11}	7.74×10^{-14}	1.51×10^{-11}

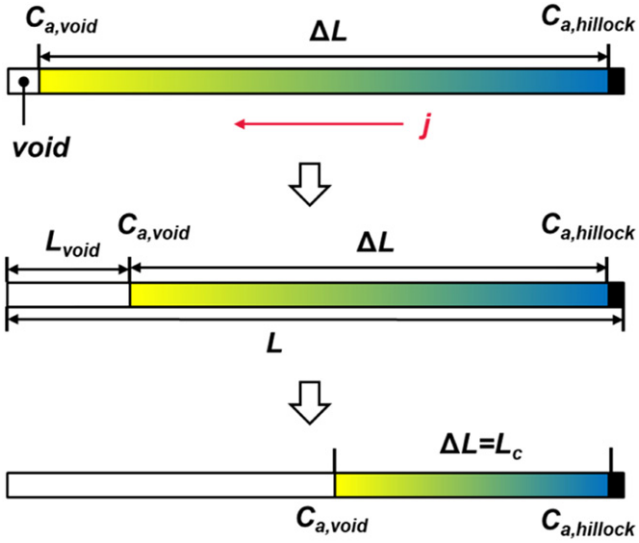

Figure 10. The schematic for the void and concentration evolutions during electromigration.

3.3.2. Effective diffusivity and grain boundary diffusivity. For different Al stripes tested at various temperatures, figures 4–6 have shown that the critical length is around 10 μm. At critical length, electromigration stops and v_{drift} is equal to zero. According to equation (7), following balance condition between electron wind and atomic concentration gradient can be obtained,

$$-Z^* e\rho j = kT\frac{\Delta C_a}{C_{a0}L_c}. \tag{11}$$

Here, we select following parameters: $e = 1.6 \times 10^{-19}$ C, $\rho = 2.88 \times 10^{-8}\ \Omega$ m, $j = -1 \times 10^{10}$ A m^{-2} [2], $k = 1.38 \times 10^{-23}$ J K^{-1}, and $L_c = 10\ \mu$m. In literature, Z^* was given from 1–10 for metals. We select $Z^* = 1$ for Al in present calculation. Based on equation (11), the difference of atomic concentration at both ends is obtained, $\Delta C_a = 0.068 C_{a0}$. Moreover, for 100 μm Al stripes, the void length and duration time are listed in table 2. Applying those parameters and $\Delta C_a = 0.068 C_{a0}$ to equation (9), the effective diffusivity for Al can be calculated, as listed in table 3 and plotted in figure 11(a).

Furthermore, to determine the grain boundary diffusivities, the parameters of H_{GBs} and δ are required. Here, we select H_{GBs} as 2.91 for Voronoi polyhedra microstructure corresponding to present Al conductors [53]. In later content, we will show that the GBs thickness changes as a function of temperature (see equation (12)) based on the MD simulation results. Applying those parameters to equation (10), we determined the average GBs diffusivity as listed in table 3 and plotted in figure 11(b).

In figure 11(b), D_{eff} has the maximum value for Al stipe with grain size ~110 nm at 350 °C. Then, D_{eff} decreases with the increasing grain size and decreasing temperature. This means that D_{eff} follows as a function of temperature and grain size, D_{eff} (T, d_{Grain}). In figure 11, the magnitude of D_{GBs} is significantly higher than D_{eff}. And, regardless of the grain size, D_{GBs} increases with increasing temperature. But, at the same temperature, D_{GBs} changes at the same level for the Al with different grain sizes. This implies that the magnitude of D_{GBs} is irrelevant to the grain size, only affected by the temperature, D_{GBs} (T). As a validation, comparsion between present diffusivities and literature results will be presented and discussed in sections 4.1 and 4.2.

4. Simulation results

4.1. Atom motion along grain boundary

We take a polycrystalline with ~10 nm grains at 600 K as an example to illustrate the diffusion features in GBs, as plotted in figure 12. Atoms in grains remain the fcc lattice structure, and atoms along GBs have the HPC or unknown lattice structures. Those atoms with HPC structure represents the dislocations in

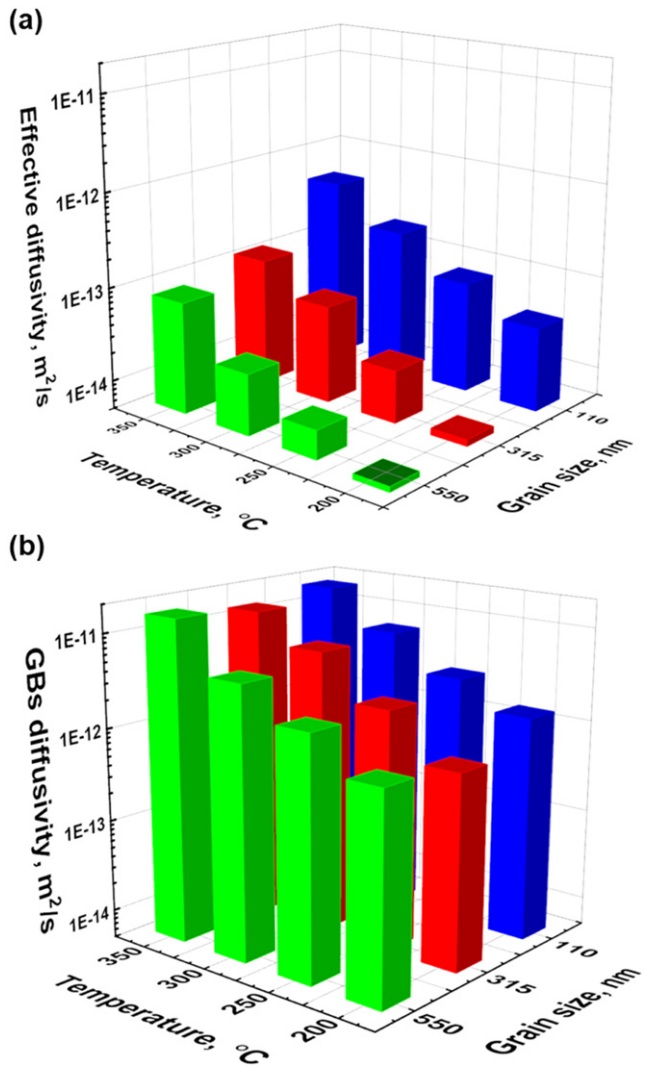

Figure 11. (a) D_{GBs} for Al with different grain size at various temperatures. (b) D_{eff} for Al with different grain size at various temperatures.

grains. Figure 6(b) plots the contour of displacement of each atom at 3.5 ns. For atoms in grains, the magnitude of displacement is very small, nearly to zero. This indicates that atoms in grains just vibrate at their own lattice sites, no diffusion happens. But, for atoms at the GBs, the magnitude of displacement is larger than a lattice distance of Al (∼3 Å), and the maximum magnitude attains 8 Å, which indicates that the atoms along GBs can jump between different lattice sites. Moreover, figure 12(c) plots the trajectory lines for the atom movements, in which the lines in GBs are dense and irregular, but trajectory lines in grains are loose and regular. These indicate that the atomic migration along GBs is more active than that in grains. Furthermore, the trajectory lines at the GBs show that the movement direction of atoms tends to along GBs. There is no apparent exchange of atoms between grain and GBs.

4.1.1. Grain boundary diffusivity. Figure 13 plots the $\mathrm{MSD}_{\mathrm{GBs}}$ at varying temperatures for the polycrystals with different grain sizes. The symbols and error bars respectively represent the average value and standard deviations among three different models at each grain size. Regardless of the grain sizes, $\mathrm{MSD}_{\mathrm{GBs}}$ is larger at higher temperatures. Although for the $\mathrm{MSD}_{\mathrm{GBS}}$ with different grain sizes at the same temperature have different error bars, the average $\mathrm{MSD}_{\mathrm{GBs}}$ changes at the same level, slightly different from each other. The MSD, as defined in equation (1), represents the average distance for atomic movement. Thus, there results in figure 13 indicates that increasing temperatures could significantly promote atomic diffusion along GBs; however, the grain size has little effect on the values of $\mathrm{MSD}_{\mathrm{GBs}}$. Here, the $\mathrm{MSD}_{\mathrm{GBs}}$ also includes some atoms in dislocations. Based on figure 12(a), the number of dislocations in grains are small part of atoms in GBs. Thus, results of $\mathrm{MSD}_{\mathrm{GBS}}$ are dominated by atoms along GBs.

According to the equation (3), GBs diffusivities for the models with different grain sizes at various temperature were calculated by using obtained $\mathrm{MSD}_{\mathrm{GBS}}$, as plotted in figure 14. The magnitude of D_{GBs} with different grain sizes are close to each other, indicating a slight effect of grain size on D_{GBs}. Moreover, based on present experimental results of D_{GBs}, an Arrhenius equation with $D_0 = 9.34 \times 10^{-8}$ m^2 s^{-1} and $E_{\mathrm{a}} = 0.474$ eV was determined (see red solid line in figure 14). Although the magnitudes of D_{GBs} from simulation approximately agree with experimental results, its slope is less than that from experiments. This indicates a lower activation energy obtained from simulation. It may be because the constrain conditions applied in the simulation are different from experiments. As Al stripes are supported on TiN in experiments, thus the atomic diffusion at the interface between Al and TiN, and the stress induced due to thermal mismatch between Al and TiN may affect the rate of mass transport. However, those influential factors are neglected in MD simulations. Moreover, the atomic diffusions along dislocations were included in the calculation of D_{GBs}, which may also cause a higher diffusivity.

Furthermore, the activation energy, 0.474 eV, determined in present study is consistent with the studies of Schreiber *et al* [35] and Mohammadzadeh *et al* [28] (see data in table 1 and curves in figure 14). But, the magnitudes of D_{GBs} in present study are higher than those given in the MD study of Mohammadzadeh *et al* After careful evaluation, the D_{GBs} calculated by Mohammadzadeh *et al* were only for twin GBs. Obviously, present MD models with random misorientation angles between grains are closer to the Al measured in experiments.

4.1.2. Grain boundary thickness. Additionally, based on the trajectory lines of the movements of the atoms, the thickness of the GB at different temperatures could be identified, as plotted in figure 15. At a low temperature (300 K), the trajectory lines along the GBs are slight and unclear, which indicates the GBs thickness is very thin and only a few atoms move along GBs. When temperature increases to 500 K, the

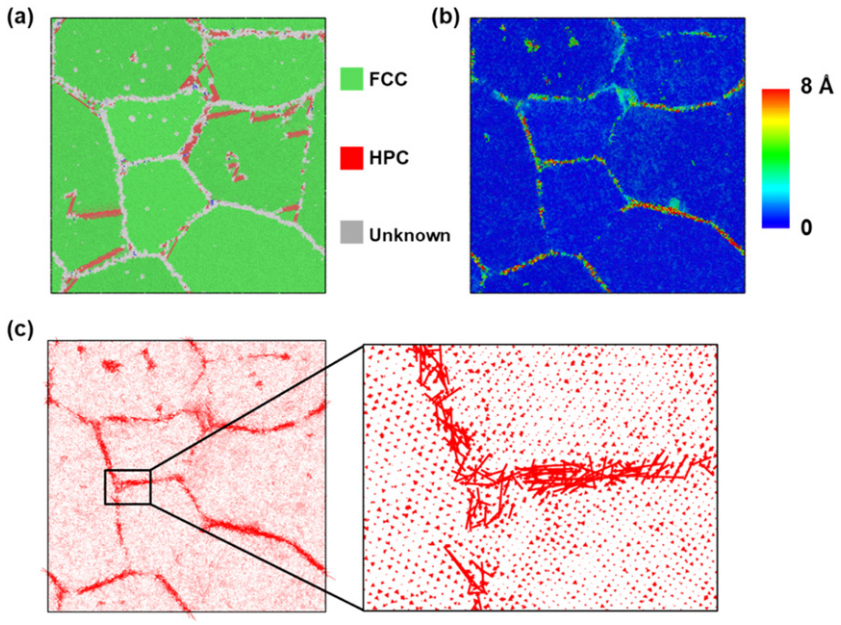

Figure 12. (a) Microstructure for the polycrystal with ∼10 nm grains at 600 K. (b) Trajectory lines for atom movements.

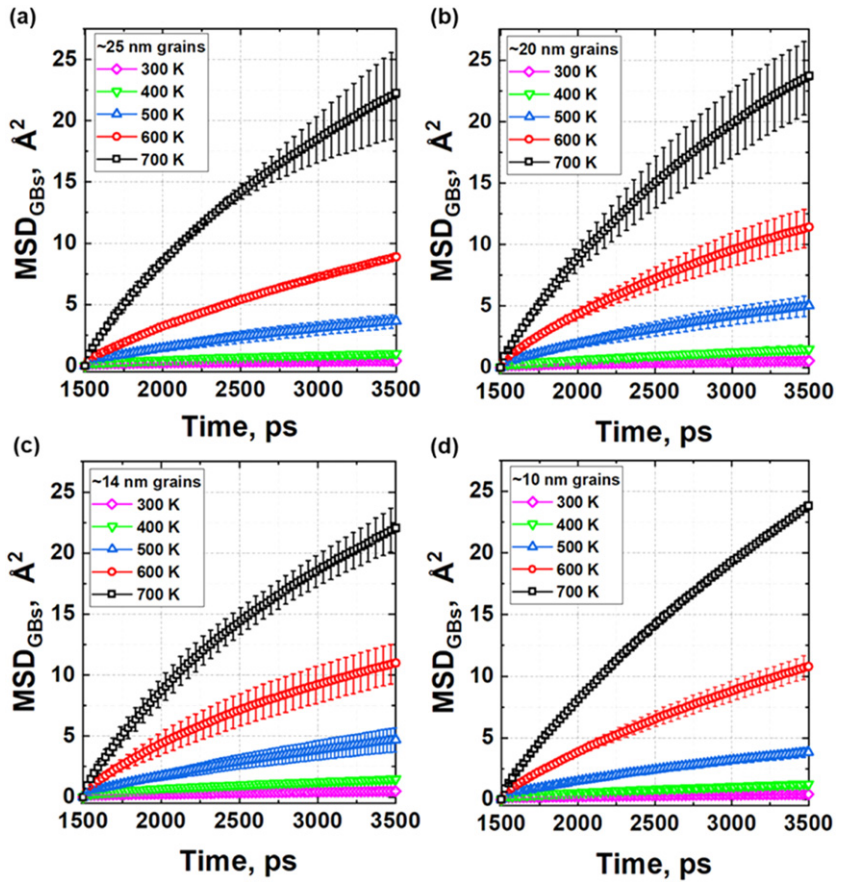

Figure 13. MSD_{GBs} at varying temperatures for the polycrystals with different grain sizes.

trajectories along the GBs become visible. At 600 K and 700 K, the outlines of trajectories along the GBs became thicker, and the thickness of GBs increases to 6.5 Å and 8 Å, respectively. As the label shown in figure 15(a) we measured the thickness of each GBs for the polycrystals at various temperature. The average values of GB thicknesses at temperatures from 300 K to 700 K are plotted in figure 15(b). The thickness of the GBs increases linearly with temperature, which is fitted as a function of temperature as follows,

$$\delta(T) = 0.015(T - 300) + 2 \tag{12}$$

where the unit of GB's thickness is Å.

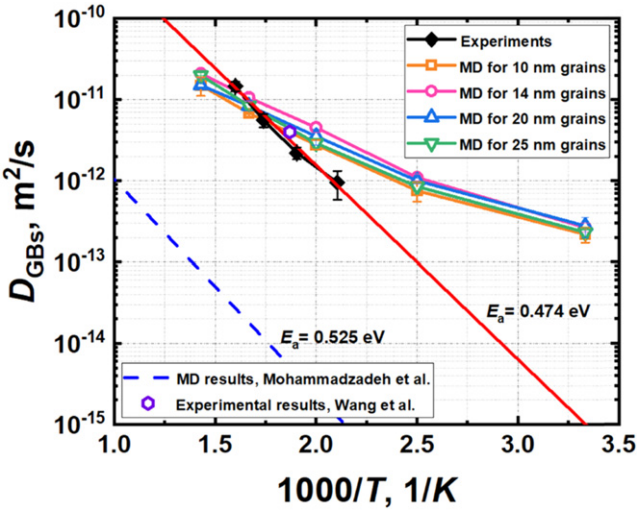

Figure 14. D_{GBs} at various temperatures for polycrystals with different grain size and the plot of Arrhenius equation.

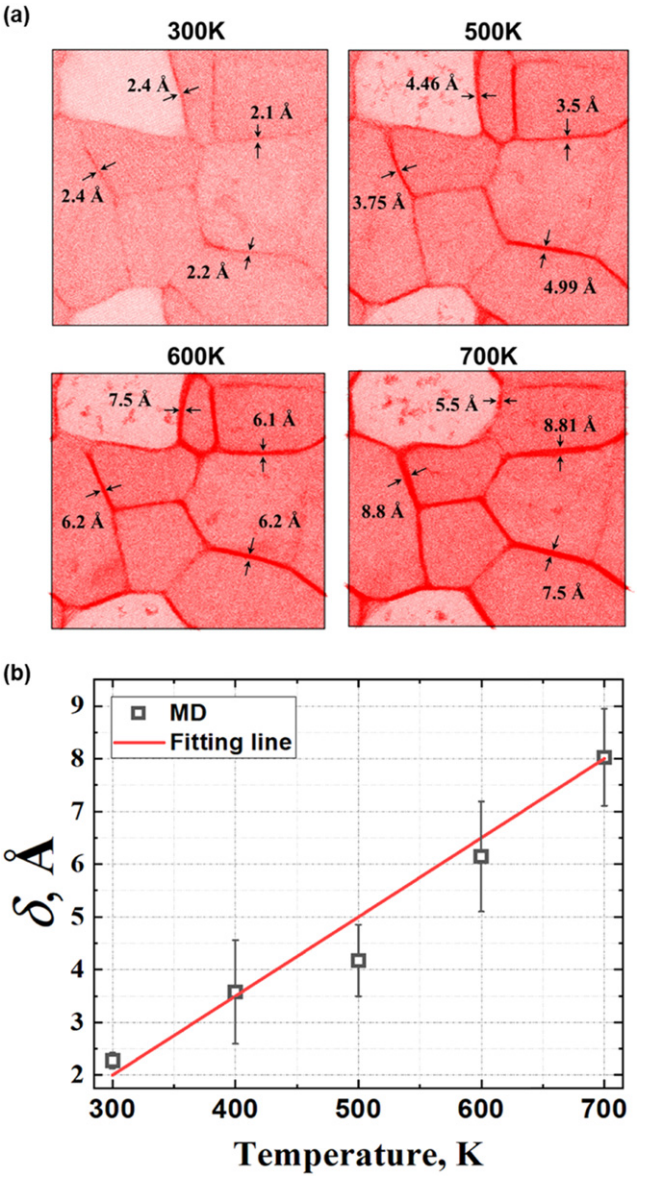

Figure 15. (a) Trajectory lines of atom movements at different temperatures for the polycrystals with ∼14 nm grains. (b) GBs thickness at various temperatures for different grain sizes.

4.2. Effective diffusivity

Effective diffusivities determined from experiments and simulations in present study are plotted in figure 16. It clearly shows that the magnitude of D_{eff} is related to the temperature and grain size. For polycrystalline with the same grain size, D_{eff} at higher temperatures is higher. At the same temperature, D_{eff} exhibited a decreasing trend with increasing grain size from 10 nm to 25 nm, from 110 nm to 550 nm. In contrast to the D_{GBs}, the magnitude of D_{eff} depends on the grain size. Moreover, our D_{eff} for Al with 110–315 nm grain sizes are agreed well with the D_{eff} determined by Fradin *et al* [30], and both studies indicated activation energy around ∼1.23 eV (see figure 14).

For the D_{eff} at the higher temperature ($T > 450$ °C), electromigration method is no longer suitable to be used to measure the diffusivities in Al, as the narrow conductor could be partially melted. Thus, we cannot obtained data at high temperatures to directly compare with the D_{eff} determined by Lundy *et al* [17]. According to the changing trend of present results, our D_{eff} seems to be significantly higher than that from Lundy. When the temperature is increased to 450 °C, the accelerated atomic diffusion along GBs would promote grain growth and simultaneously change the mechanical stress inside the material. Commonly, the temperature of 450 °C is used to annealing Al to reduce the defects and obtain a denser microstructure, producing a more stable Al film. These physical processes induced by increasing temperature may affect the determination of diffusivity in Al, causing the gap between both results.

In addition, for the D_{eff} at the low temperature ($T < 200$ °C), the activation energy of 1.31 eV was obtained in the study of Volin *et al* [32], which is a little bit higher than present results (1.23 eV). But, the changing trend of present results is qualitatively consistent with results of Volin. Actually, to determine D_{eff} at the low temperature using electromigration method, a longer duration is needed, and a suitable current density is required to avoid the joule heating effect. This part will be investigated in our future study.

In total, present D_{eff} was consistent with literature results, and a more comprehensive result of D_{eff} related to the grain size of Al was presented. Obviously, blindly selecting an effective diffusivity without considering grain size would cause significant errors. Especially for the metal used in microscale, as the sensitivity of grain size on D_{eff} would increase with decreasing grain size. Except that, present MD simulation simplified the mass transport in polycrystalline Al, to emphasize the influences from GBs and temperatures. Thus, the effects of mechanical stress, dislocations, voids, and interfacial diffusion along TiN were neglected in simulations. But, the gap between MD results and experimental results indicates that those influential factors might play an important role in accurately predicting diffusivities.

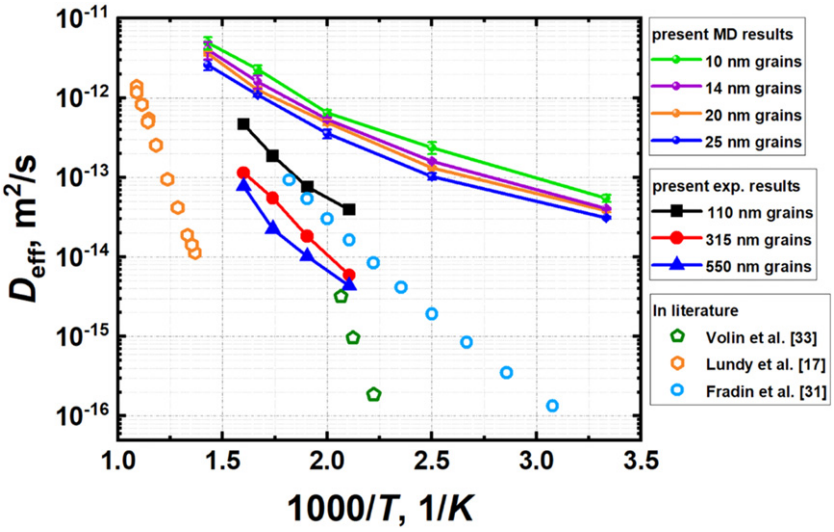

Figure 16. Present D_{eff} at various temperatures for Al with different grain size, and the comparison with literature results.

5. Conclusion

In this paper, the effects of grain size and temperature on diffusivity of polycrystalline Al were investigated via electromigration experiments and MD simulation. It was observed that the development of electromigration increases with increasing temperature and decreasing grain size. According to the electromigration results, the effective diffusivity (D_{eff}) and grain boundary diffusivity (D_{GBs}) in Al stripes were determined. It was shown that D_{eff} changes as a function of grain size and temperature, but D_{GBs} is independent of the grain size, only affected by temperature. Based on MD and experimental results, Arrhenius equation for D_{GBs} with the activation energy of 0.474 eV and activation energy of 1.23 eV for D_{eff} were determined. In total, present D_{GBs} and D_{eff} are consistent with literature results, and a more comprehensive results of diffusivities related to the grain size of Al was presented.

Acknowledgments

The authors would like to thank the staff of the Else Kooi Laboratory for processing support.

Authorship contribution statement

Zhen Cui: conceptualization, computation, data analysis, writing—review & editing. **Yaqian Zhang**: experiment, writing—review & editing. **Dong Hu**: experimental characterization, writing—review & editing. **Sten Vollebregt:** experiment, writing—review & editing. **Jiajie Fan**: writing—review & editing. **Xuejun Fan:** conceptualization, data analysis, writing—review & editing. **Guoqi Zhang:** writing—review & editing.

Data availability statement

All data that support the findings of this study are included within the article (and any supplementary files).

ORCID iDs

Zhen Cui https://orcid.org/0000-0002-0191-1194
Yaqian Zhang https://orcid.org/0000-0003-3426-3143
Sten Vollebregt https://orcid.org/0000-0001-6012-6180
Guoqi Zhang https://orcid.org/0000-0002-8023-5170

References

[1] Cui Z, Fan X and Zhang G 2019 General coupling model for electromigration and one-dimensional numerical solutions *J. Appl. Phys.* **125** 105101
[2] Black J R 1969 Electromigration-a brief survey and some recent results *IEEE Trans. Electron Devices* **16** 338–47
[3] Satake T, Yokoyama K, Shirakawa S and Sawaguchi K 1973 Electromigration in aluminum film stripes coated with anodic aluminum oxide films *Jpn. J. Appl. Phys.* **12** 518
[4] Tseng I-H, Hsu P-N, Lu T-L, Tu K N and Chen C 2021 Electromigration failure mechanisms of ⟨111⟩-oriented nanotwinned Cu redistribution lines with polyimide capping *Res. Phys.* **24** 104154
[5] Spigarelli S and Sandström R 2018 Basic creep modelling of aluminium *Mater. Sci. Eng.* A **711** 343–9
[6] Yamakov V, Wolf D, Phillpot S R and Gleiter H 2002 Grain-boundary diffusion creep in nanocrystalline palladium by molecular-dynamics simulation *Acta Mater.* **50** 61–73
[7] Long X, Tang W, Xu M, Keer L M and Yao Y 2018 Electric current-assisted creep behaviour of Sn-3.0Ag-0.5Cu solder *J. Mater. Sci.* **53** 6219–29
[8] Long X, He X and Yao Y 2017 An improved unified creep-plasticity model for SnAgCu solder under a wide range of strain rates *J. Mater. Sci.* **52** 6120–37
[9] Ashby M F 1974 A first report on sintering diagrams *Acta Metall.* **22** 275–89

[10] Hu D, Cui Z, Fan J, Fan X and Zhang G 2020 Thermal kinetic and mechanical behaviors of pressure-assisted Cu nanoparticles sintering: a molecular dynamics study *Res. Phys.* **19** 103486

[11] Long X, Jia Q P, Li Z and Wen S X 2020 Reverse analysis of constitutive properties of sintered silver particles from nanoindentations *Int. J. Solids Struct.* **191–192** 351–62

[12] Long X, Jia Q, Shen Z, Liu M and Guan C 2021 Strain rate shift for constitutive behaviour of sintered silver nanoparticles under nanoindentation *Mech. Mater.* **158** 103881

[13] Gilmer G H, Huang H and Roland C 1998 Thin film deposition: fundamentals and modeling *Comput. Mater. Sci.* **12** 354–80

[14] Budke E, Surholt T, Prokofjev S I, Shvindlerman L S and Herzig C 1999 Tracer diffusion of Au and Cu in a series of near $\Sigma = 5$ (310)[001] symmetrical Cu tilt grain boundaries *Acta Mater.* **47** 385–95

[15] Seeger A, Wolf D and Mehrer H 1971 Analysis of tracer and nuclear magnetic resonance measurements of self-diffusion in aluminium *Phys. Status Solidi b* **48** 481–96

[16] Demmel F, Szubrin D, Pilgrim W-C and Morkel C 2011 Diffusion in liquid aluminium probed by quasielastic neutron scattering *Phys. Rev.* B **84** 014307

[17] Lundy T S and Murdock J F 1962 Diffusion of Al^{26} and Mn^{54} in aluminum *J. Appl. Phys.* **33** 1671–3

[18] Balluffi R W 1982 Grain boundary diffusion mechanisms in metals *Metall. Trans.* B **13** 527–53

[19] Peterson N L 1983 Grain-boundary diffusion in metals *Int. Met. Rev.* **28** 65–91

[20] Sakaguchi I, Yurimoto H and Sueno S 1992 Self-diffusion along dislocations in single-crystals MgO *Solid State Commun.* **84** 889–93

[21] Nakagawa T, Nakamura A, Sakaguchi I, Shibata N, Lagerlöf K P D, Yamamoto T, Haneda H and Ikuhara Y 2006 Oxygen pipe diffusion in sapphire basal dislocation *J. Ceram. Soc. Japan* **114** 1013–7

[22] Zhu A, Kê T and Tingsui G 1991 Activation energy associated with the nonlinear internal friction peak around room temperature in cold-worked Al-0.1 wt% Cu *Phys. Status Solidi a* **128** 95–102

[23] Blech I A 1998 Diffusional back flows during electromigration *Acta Mater.* **46** 3717–23

[24] Wang Z M and Shiflet G J 1998 Growth of δ' on dislocations in a dilute Al–Li alloy *Metall. Mater. Trans.* A **29** 2073–85

[25] Sandberg N, Magyari-Köpe B and Mattsson T R 2002 Self-diffusion rates in Al from combined first-principles and model-potential calculations *Phys. Rev. Lett.* **89** 065901

[26] Jakse N and Pasturel A 2013 Liquid Aluminum: atomic diffusion and viscosity from *ab initio* molecular dynamics *Sci. Rep.* **3** 1–8

[27] Suzuki A and Mishin Y 2005 Atomic mechanisms of grain boundary diffusion: low versus high temperatures *J. Mater. Sci.* **40** 3155–61

[28] Mohammadzadeh M and Mohammadzadeh R 2017 Effect of grain size on apparent diffusivity in nanocrystal α-iron by atomistic simulation *Comput. Mater. Sci.* **129** 239–46

[29] Kargl F, Weis H, Unruh T and Meyer A 2012 Self diffusion in liquid aluminium *J. Phys.: Conf. Ser.* **340** 012077

[30] Fradin F Y and Rowland T J 1967 NMR measurement of the diffusion coefficient of pure aluminum *Appl. Phys. Lett.* **11** 207–9

[31] Stoebe T G and Dawson H I 1968 Analysis of self-diffusion and quenching studies in aluminum and gold *Phys. Rev.* **166** 621

[32] Volin T E and Balluffi R W 1968 Annealing kinetics of voids and the Self-diffusion coefficient in aluminum *Phys. Status Solidi b* **25** 163–73

[33] Burke J and Ramachandran T R 1972 Self-diffusion in aluminum at low temperatures *Metall. Mater. Trans.* B **3** 147–55

[34] Levenson L L 1989 Grain boundary diffusion activation energy derived from surface roughness measurements of aluminum thin films *Appl. Phys. Lett.* **55** 2617–9

[35] Schreiber H-U and Grabe B 1981 Electromigration measuring techniques for grain boundary diffusion activation energy in aluminum *Solid-State Electron.* **24** 1135–46

[36] Wang P-C, Cargill G S III, Noyan I C and Hu C-K 1998 Electromigration-induced stress in aluminum conductor lines measured by x-ray microdiffraction *Appl. Phys. Lett.* **72** 1296–8

[37] Sørensen M R, Mishin Y and Voter A F 2000 Diffusion mechanisms in Cu grain boundaries *Phys. Rev.* B **62** 3658

[38] Zhang Y 2019 Experimental study of electromigration using Blech's structure *Master Thesis* Delft University of Technology

[39] Voter A F 1993 Embedded atom method potentials for seven fcc metals: Ni, Pd, Pt, Cu, Ag, Au, and Al *Los Alamos Unclassified Technical Report LA-UR 93-3901* Los Alamos National Laboratory

[40] Holm E A, Olmsted D L and Foiles S M 2010 Comparing grain boundary energies in face-centered cubic metals: Al, Au, Cu and Ni *Scr. Mater.* **63** 905–8

[41] Asta M, Morgan D, Hoyt J J, Sadigh B, Althoff J D, De Fontaine D and Foiles S M 1999 Embedded-atom-method study of structural, thermodynamic, and atomic-transport properties of liquid Ni–Al alloys *Phys. Rev.* B **59** 14271

[42] Brostow W, Dussault J-P and Fox B L 1978 Construction of Voronoi polyhedra *J. Comput. Phys.* **29** 81–92

[43] Finney J L 1979 A procedure for the construction of Voronoi polyhedra *J. Comput. Phys.* **32** 137–43

[44] Stukowski A 2009 Visualization and analysis of atomistic simulation data with OVITO-the open visualization tool *Modelling Simul. Mater. Sci. Eng.* **18** 015012

[45] Sellers M S, Schultz A J, Basaran C and Kofke D A 2010 β-Sn grain-boundary structure and self-diffusivity via molecular dynamics simulations *Phys. Rev.* B **81** 134111

[46] Rao Z, Wang S and Peng F 2013 Self diffusion and heat capacity of n-alkanes based phase change materials: a molecular dynamics study *Int. J. Heat Mass Transfer* **64** 581–9

[47] Annamareddy A, Voyles P M, Perepezko J and Morgan D 2021 Mechanisms of bulk and surface diffusion in metallic glasses determined from molecular dynamics simulations *Acta Mater.* **209** 116794

[48] Pun G P and Mishin Y 2009 A molecular dynamics study of self-diffusion in the cores of screw and edge dislocations in aluminum *Acta Mater.* **57** 5531–42

[49] Tan C M and Roy A 2007 Electromigration in ULSI interconnects *Mater. Sci. Eng.* R **58** 1–75

[50] Chen C, Hsiao H-Y, Chang Y-W, Ouyang F and Tu K-N 2012 Thermomigration in solder joints *Mater. Sci. Eng.* R **73** 85–100

[51] Zhang P, Xue S and Wang J 2020 New challenges of miniaturization of electronic devices: electromigration and thermomigration in lead-free solder joints *Mater. Des.* **19** 108726

[52] Hart E W 1957 On the role of dislocations in bulk diffusion *Acta Metall.* **5** 597

[53] Chen Y and Schuh C A 2007 Geometric considerations for diffusion in polycrystalline solids *J. Appl. Phys.* **101** 063524

[54] Thorvaldsen A 1997 The intercept method—2. Determination of spatial grain size *Acta Mater.* **45** 595–600

[55] Thorvaldsen A 1997 The intercept method—1. Evaluation of grain shape *Acta Mater.* **45** 587–94